DFT/TDDFT study of ground and low-lying excited states of $Fe_2(S_2C_3H_6)(CO)_6$, a simple functional model of the [FeFe]-hydrogenase active site - Supplementary materials

Luca Bertini, Claudio Greco, Luca De Gioia, Piercarlo Fantucci

Department of Biotechnology and Biosciences

Universita' degli Studi di Milano-Bicocca

Piazza della Scienza, 2; 20126 Milan - Italy

To whom correspondence should be addressed:

Dr. Luca Bertini email: luca.bertini@unimib.it

Prof. Piercarlo Fantucci email:piercarlo.fantucci@unimib.it

March 10, 2009

Outline

1. On the multireference character of the **a** stationary point wavefunctions

2. Analysis of the Frontier Molecular orbitals (FMO)

3. BP86 and B3LYP CO stretching modes

4. ^{1}**a** excitation energies as a function of the DFT functional

1 On the multireference character of the a stationary point wavefunctions

The DFT approach has been successfully applied to transition metal complexes, with a semi-quantitative agreement with the experimental data, in particular when equilibrium geometries or the characterization of reaction paths are concerned. However, the monodeterminantal description of DFT method is not fairly adapted to describe electronic structures with a significant multireference character.[3] In order to evaluate the multireference character of the singlet stationary point wavefunctions, single points energy computations using Complete Active Space SCF (CAS) were employed with a necessarily small active space (see Table). Complete active space (CAS) single point energy computations were carried out with TZVP basis set using Gaussian03 [1] suite of programs. A first set of calculations were carried out using CAS(4,4)/TZVP (20 configurations). At this level of theory, B3LYP geometries are lower in energy with respect to BP86 (-0.0863 hartree for ^{1}**a**, -0.0375 hartree $^1\mathbf{a}_{syn}$, -0.0338 hartree $^1\mathbf{a}_{anti}$). A similar result was also found in CCSD singlet point energy computations for $Fe_2(CO)_8$.[2] A second set of calculations were carried out on B3LYP optimized geometries at CAS(8,8)/TZVP level of theory

Table 1: Single point Restricted Hartree-Fock (RHF) and Complete active space SCF (CAS) energy computations on BP86 and B3LYP singlet ground state PES stationary points.

Geometry	Level	${}^1\mathbf{a}^{(b)}$	${}^1\mathbf{a}_{syn}{}^{(b)}$	${}^1\mathbf{a}_{anti}{}^{(b)}$	$\delta_{syn}{}^{(c)}$	$\delta_{anti}{}^{(c)}$
BP86	RHF	-4113.3927	-4113.3469	-4113.3387		
	CAS(4,4)$^{(a)}$	-4113.4214	-4113.3940	-4113.3837	16.9	23.7
B3LYP	RHF	-4113.4294	-4113.3824	-4113.3747		
	CAS(4,4)$^{(a)}$	-4113.5078	-4113.4325	-4113.4174	47.3	56.7
	CAS(8,8)$^{(a)}$	-4113.5771	-4113.5730	-4113.5648	3.7	8.2

$^{(a)}$ CAS(n,m) where n and m refer to the number MOs and number of electron included in the active space; $^{(b)}$ Energies in hartree; $^{(c)}$ Energies in kcal·mol^{-1}

(1764 configurations). The occupation numbers of the active orbitals of the all-terminal CO structure are 1.999, 1.926, 1.927, 1.891, 0.110, 0.072, 0.072 and 0.0001, attesting a not dramatic multireference character of the single determinant wavefunctions. A similar result is also found in the case of the two transition states (1.918, 1.914, 1.998, 1.881, 0.112, 0.082, 0.086 and 0.0007 syn, 1.999, 1.914, 1.916, 1.892, 0.109, 0.083, 0.082 and 0.0002 $anti$). The energy differences between rotated and all terminal CO structures computed at CAS(8,8) level are lower then those obtained at DFT level. Although the quality of these CAS computations could be improved, since the dynamical correlation is largely neglected and no geometry optimization has been performed, the DFT level seems appropriate in describing these systems.

Table 2: **a** Frontier molecular orbital composition analysis at BP86/TZVP level of theory.

MO	irrep	Energy (hartree)	%				
			2Fe	2S	2 cis CO	4 $trans$ CO	$(CH_2)_3$
LUMO+3	$63a'$	-0.082	15.9	11.9	16.0	46.3	9.9
LUMO+2	$37a''$	-0.110	17.0	24.2	6.2	35.4	17.2
LUMO+1	$36a''$	-0.113	20.7	21.8	7.3	35.1	15.0
LUMO	$62a'$	-0.130	31.4	12.2	26.2	18.2	12.0
HOMO	$61a'$	-0.223	37.7	12.8	32.8	12.8	8.3
HOMO-1	$60a'$	-0.232	40.5	10.6	13.9	28.5	9.0
HOMO-2	$35a''$	-0.234	28.3	19.1	15.0	28.7	9.9
HOMO-3	$34a''$	-0.239	38.4	10.7	8.8	31.6	4.4
HOMO-4	$59a'$	-0.240	32.2	15.3	11.0	31.0	12.7

The % orbital compositions are reported as sum of the individual atomic composition of a givel set of atoms. 2Fe and 2S refers to the sum of the atomic arbital composition of the two Fe atom and the two S atoms. Similarly is reported for the CO ligands (two cis and found $trans$) and the alkyl chain of the pdt.

2 Analysis of the Frontier Molecular orbitals (FMO)

We discuss the shapes and relative energies of the BP86 FMO of all the structures considered. The shape of the ^{1}**a** FMO are reported in figure 1. The FMO correlation diagrams for **a**, $\mathbf{a}^-$ and $\mathbf{a}^+$ specie are shown in figure 2. In order to simplify the correlation energy diagrams for the doublet state systems, we newly computed energies and wavefunctions at ROBP86 level.

Let us first consider the FMO of the stationary points on the ^{1}**a** PES. These MOs have been already characterized in detail in previous papers [5, 6, 7, 8, 4], but in order to better discuss the following results it is important to recall that the HOMO ($61a'$) has a large lobe slightly below the Fe-Fe internuclear axes (Fe-Fe $bent$ bond) and it has a σ Fe-Fe bonding character. On the contrary, the LUMO ($62a'$) has Fe-Fe σ^* antibonding character. The FMO correlation diagram shows the decreased HOMO/LUMO gap in $^1\mathbf{a}_{syn}$ (0.0686 hartree) and $^1\mathbf{a}_{anti}$ (0.0651 hartree) compared with that of ^{1}**a** (0.0925 hartree). These two MOs have Fe-Fe bonding and antibonding character, but also a strong Fe-C_μ bonding [12] and antibonding/nonbonding character, respectively. The FMO shapes of the all-terminal and rotated forms on the cationic and anionic PES do not change significantly compared with that of the neutral forms. Regarding the cationic PES, the destabilization of the SOMO for the rotated structures is lower ($anti$ 0.016 hartree, syn 0.0095 hartree) than that of the HOMO of the corresponding neutral forms ($anti$ 0.021 hartree, syn 0.019 hartree), contributing to the stabilization of the formers. The main features of the MO from HOMO-1 to HOMO-4 are the same in the all-terminal and rotated structures: HOMO-1 (35a$''$), HOMO-2 (34a$''$) and HOMO-4 (59a$'$) are mainly characterized by a d-Fe p-S bonding orbital combination, while HOMO-3 (60a$'$) has a strong Fe-C_{cis} bonding character. In the all-terminal structure the HOMO-1/HOMO-2 and HOMO-3/HOMO-4 form two couples of almost degenerate MO, and this degeneracy is broken in the rotated structures due to the asymmetry between the $anti$ and syn iron and sulfur atoms. Finally, the LUMO+1 (36a$''$) and LUMO+2 (37a$''$) have syn and $anti$ Fe-C_{trans} and Fe-S antibonding character, respectively.

In Table 2 are reported the orbital composition analysis of the MO going from the HOMO-4 to the LUMO+3. All occupied MOs considered are characterized by a larger contribution of the Fe orbitals and a smaller contribution of the S orbitals compared to virtual MOs.

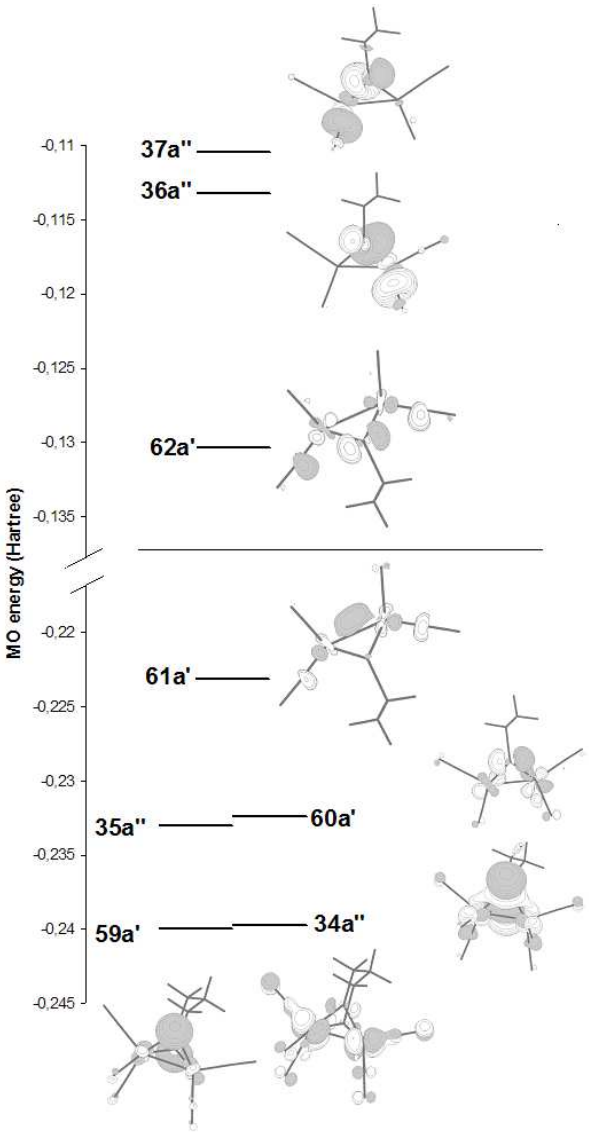

Figure 1:Frontier molecular orbital energy diagrams and shapes for the ^{1}**a**. Orbital energies in hartree

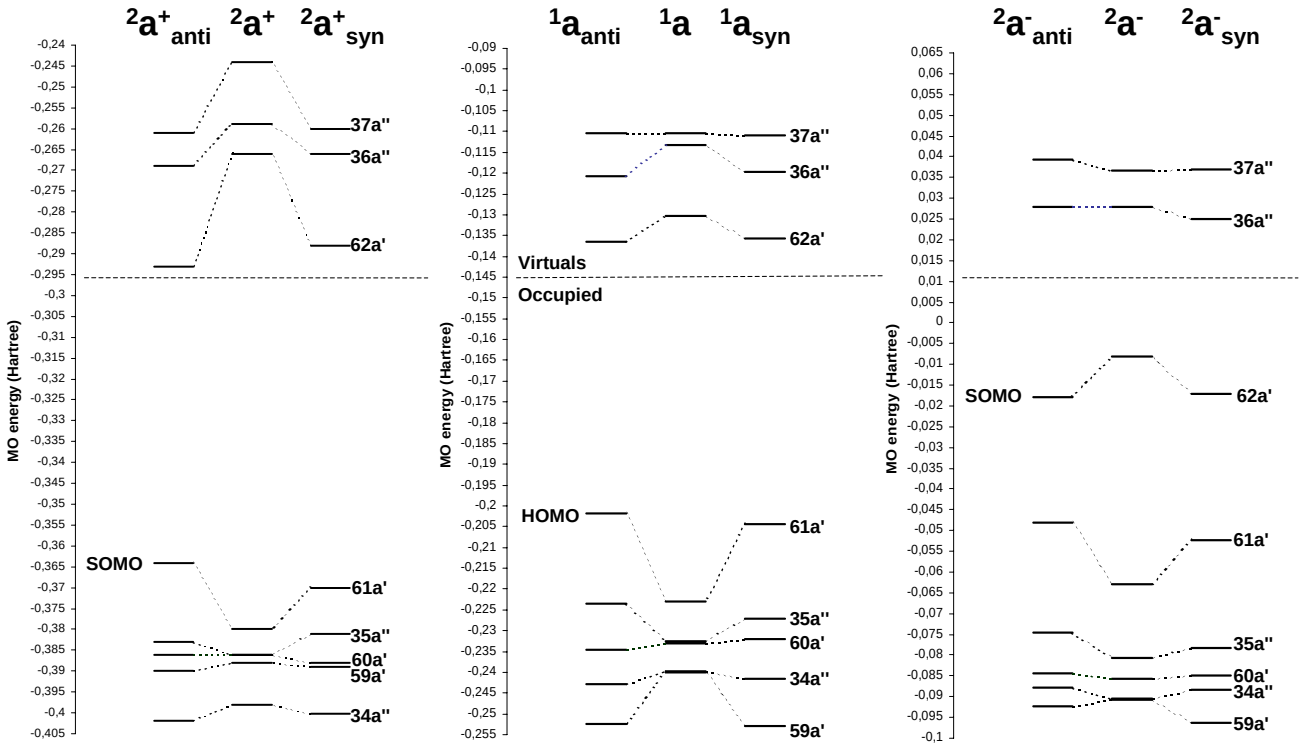

Figure 2: ROBP86 frontier molecular orbital correlation diagrams for the **a**, $\mathbf{a}^+$ and $\mathbf{a}^-$ PES stationary points found. Orbital energies in hartree

3 BP86 and B3LYP CO stretching modes

In table 3 and 4 are reported the BP86 and B3LYP CO stretching modes for all the gropund state specie investigated in this paper (**a** and its cationic and anionic forms, in the all-terminal, syn and $anti$ forms. BP86 frequencies are slightly closer to the experimental values and are characterized by a sum of the absolute errors $\sum_i |\nu_{exp,i} - \nu_{calc,i}|$ equal to 24 cm^{-1}, while the corresponding value for B3LYP is 42 cm^{-1}. The profile of the IR spectra in the CO stretching modes region is similar to that of **a**, with all frequencies decreased by roughly 70 cm^{-1}. On average, $^2\mathbf{a}^-$ BP86 values are lower by 81 cm^{-1} with respect to $^1\mathbf{a}$ values.

Table 3: **a** computed CO stretching mode frequencies.

a	exp$^{(a)}$	BP86 freq$^{(b)}$ (int.$^{(c)}$)	B3LYP freq$^{(b)}$ (int.$^{(c)}$)
a'	1971	1978 (308)	1988 (126)
a'	1993	1986 (815)	1997 (908)
a''		1986 (3)	1994 (1)
a''	2000	2003 (1105)	2011 (1289)
a'	2028	2028 (1445)	2019 (2315)
a'	2064	2064 (521)	2066 (608)
sum$^{(c)}$		24	42

$^{(a)}$ see ref.[9]; $^{(b)}$ stretching CO frequency in cm^{-1}; B3LYP frequencies are scaled by a 0.9614 factor see [11]; $^{(c)}$ IR intensity in km·mol^{-1}; $^{(d)}$ sum = $\sum_i |\nu_{exp,i} - \nu_{computed,i}|$ in cm^{-1}.

Table 4: $\mathbf{a}^+$ and $\mathbf{a}^-$ BP86 computed CO stretching normal mode frequencies.

	$^2\mathbf{a}^+$	$^2\mathbf{a}^+_{anti}$	$^2\mathbf{a}^+_{syn}$
	freq$^{(a)}$ (int.$^{(b)}$)	freq$^{(a)}$ (int.$^{(b)}$)	freq$^{(a)}$ (int.$^{(b)}$)
	2035 (207)	2006 (266)	1992 (283)
	2041 (672)	2047 (482)	2048 (473)
	2050 (34)	2055 (338)	2056 (334)
	2058 (855)	2063 (584)	2065 (588)
	2081 (1235)	2019 (1281)	2085 (1268)
	2106 (394)	2066 (364)	2111 (338)
exp$^{(c)}$	$^2\mathbf{a}^-$	$^2\mathbf{a}^-_{anti}$	$^2\mathbf{a}^-_{syn}$
	freq$^{(a)}$ (int.$^{(b)}$)	freq$^{(a)}$ (int.$^{(b)}$)	freq$^{(a)}$ (int.$^{(b)}$)
1880	1886 (1212)	1891 (921)	1896 (719)
1905	1893 (901)	1899 (659)	1901 (654)
	1912 (20)	1903 (659)	1905 (749)
1925	1928 (1409)	1928 (838)	1925 (847)
1950 s	1946 (1486)	1942 (2072)	1943 (2188)
2010	1994 (783)	1993 (706)	1992 (675)

$^{(a)}$ stretching CO frequency in cm^{-1}; $^{(b)}$ IR intensity in km·mol^{-1}; $^{(c)}$ Experimental values for $^2\mathbf{a}^-$. See ref.[9]

4 ^{1}a excitation energies as a function of the DFT functional.

We calculated the excitation energies for $^1\mathbf{a}$ using BP86, B3LYP and PBE0 DFT functional. In the table below we considered the comparison between the values obtained using the three DFT functionals for a selection of excitation relevant to the UV-Vis spectra. In particular the $1^1A''$ is the lowest wevelenght absorption according to all the functional considered. The $2^1A'$ excitation correspond to the weak intensity shoulder, found at 461 nm.[4] Finally $3^1A'$ and $4^1A'$ correspond to the intense band center at 327-329 nm. According to the orbital composition analysis for the FMO, the UV-Vis spectra transitions are mainly characterized by a reorganization of the electron density. On average the virtual FMO considered (see table 2) has a smaller Fe orbital contribution and an higher S orbital contribution compared to the occupied FMO, and therefore the majority of the electronic transitions have a small metal-to-ligands CT character.

The results obtained using the three DFT functionals are all in qualitative agreement with the experimental results. Considering the $2^1A'$ band as the center of weak shoulder at 461 nm, BP86 excitation energy results in better agreement with the experimental values with respect to B3LYP and PBE0. According to the discussion of the UV-vis experimental spectra[4], the $3^1A'$ and $4^1A'$ transitions are assigned to the intense band centered at 327-329 nm. For all DFT functional considered, the excitation energies results understimated, and PBE0 ones are in better agreement with the experimental values (underestimated by 0.15-0.25 eV), followed by B3LYP and BP86 results (underestimated by 0.36-0.47 and 0.42-0.57, respectively).

Finally, the state composition obtained using hybrid functionals is different form that found using pure GGA BP86. This results, as well as the counterintuitive fact that HOMO→LUMO transition is not the lowest energy excitation, can be justified by the lack of molecular orbital relaxation within the TDDFT computations.[4] In order to partially show the effect of the orbital relaxation on the excitation energies, we compute the vertical energy difference between the **a** ground state and the 1^1A$''$ excited state at the **a** ground state geometry. This is possible at DFT level for this particular case by changing the MO occupancy from $35a''(2)60a''(2)61a''(2)62a''(0)$ to $35a''(1)60a''(2)61a''(2)62a''(1)$ and imposing the C$_s$ molecular symmetry. The excitation energy at BP86 lebel of theory goes from 434.1 nm to 454.5 nm.

Table 5: Selected ^{1}**a** computed excitation energies and state compositions as a function of the DFT functional (BP86, B3LYP and PBE0).

State	Functional	nm$^{(a)}$	eV$^{(a)}$	1e$^{(b)}$
$1^1A''$	BP86	434.1		97.5 $35a'' \rightarrow 62a'$
	B3LYP	427.1		79.7 $34a'' \rightarrow 62a'$
	PBE0	402.4		78.7 $34a'' \rightarrow 62a'$
$2^1A'$	BP86	408.7	3.03	54.9 $59a' \rightarrow 62a'$
				23.4 $61a' \rightarrow 62a'$
				13.4 $60a' \rightarrow 62a'$
	B3LYP	391.8	3.16	57.0 $61a' \rightarrow 62a'$
				21.4 $59a' \rightarrow 62a'$
	PBE0	362.9	3.41	55.7 $61a' \rightarrow 62a'$
				24.4 $59a' \rightarrow 62a'$
	exp$^{(c)}$	461	2.69	
$3^1A'$	BP86	382.3	3.24	31.2 $59a' \rightarrow 62a'$
				13.2 $61a' \rightarrow 62a'$
				11.4 $35a'' \rightarrow 37a''$
	B3LYP	375.5	3.30	30.8 $58a' \rightarrow 62a'$
				19.9 $57a' \rightarrow 62a'$
				10.3 $61a' \rightarrow 62a'$
				9.9 $35a'' \rightarrow 36a''$
	PBE0	351.7	3.52	26.5 $58a' \rightarrow 62a'$
				25.8 $59a' \rightarrow 62a'$
				6.6 $35a'' \rightarrow 37a''$
	exp$^{(c)}$	327	3.77	
$4^1A'$	BP86	369.9	3.35	63.5 $58a' \rightarrow 62a'$
				16.2 $57a' \rightarrow 62a'$
	B3LYP	363.5	3.41	46.7 $59a' \rightarrow 62a'$
				20.4 $58a' \rightarrow 62a'$
				8.8 $61a' \rightarrow 62a'$
				7.7 $60a' \rightarrow 62a'$
	PBE0	342.4	3.62	42.1 $59a' \rightarrow 62a'$
				15.4 $58a' \rightarrow 62a'$
				14.8 $61a' \rightarrow 62a'$
				9.2 $60a' \rightarrow 62a'$
	exp$^{(c)}$	327	3.77	

$^{(a)}$ nm and eV are the excitation energies in nm or eV;
$^{(b)}$ the leading one-electron excitation refers to the single-excitation contribution $a \rightarrow i$;
$^{(c)}$ ref. [4]. Experimental values are reported according to the assignment made in the text.

References

[1] M. J. Frisch, G. W. Trucks, H. B. Schlegel, G. E. Scuseria, M. A. Robb, J. R. Cheeseman, J. A. Montgomery Jr, T. Vreven, K. N. Kudin, J. C. Burant, J. M. Millam, S. S. Iyengar, J. Tomasi, V. Barone, B. Mennucci, M. Cossi, G. Scalmani, N. Rega, G. A. Petersson, H. Nakatsuji, M. Hada, M. Ehara, K. Toyota, R. Fukuda, J. Hasegawa, M. Ishida, T. Nakajima, Y. Honda, O. Kitao, H. Nakai, M. Klene, X. Li, J. E. Knox, H. P. Hratchian, J. B. Cross, V. Bakken, C. Adamo, J. Jaramillo, R. Gomperts, R. E. Stratmann, O. Yazyev, A. J. Austin, R. Cammi, C. Pomelli, J. W. Ochterski, P. Y. Ayala, K. Morokuma, G. A. Voth, P. Salvador, J. J. Dannenberg, V. G. Zakrzewski, S. Dapprich, A. D. Daniels, M. C. Strain, O. Farkas, D. K. Malick, A. D. Rabuck, K. Raghavachari, J. B. Foresman, J. V. Ortiz, Q. Cui, A. G. Baboul, S. Clifford, J. Cioslowski, B. B. Stefanov, G. Liu, A. Liashenko, P. Piskorz, I. Komaromi, R. L. Martin, D. J. Fox, T. Keith, M. A. Al-Laham, C. Y. Peng, A. Nanayakkara, M. Challacombe, P. M. W. Gill, B. Johnson, W. Chen, M. W. Wong, C. Gonzalez and J. A. Pople, GAUSSIAN 03 (Revision C.02), Gaussian, Inc., Wallingford CT, 2004.

[2] Bertini, L.; Bruschi, M.; De Gioia, L.; Fantucci, P.; *J. Phys. Chem. A*, **2007**, *111*, 12152

[3] Platts, J.A. and Evans, G.J.S. and Coogan, M.P. and Overgaard, J. *Inorg. Chem. 46* **2007**, 6291

[4] Fiedler, A. T.; Brunold, T. C. *Inorg. Chem.* **2005**, *44*, 1794

[5] Yang, X.; Razavet, M.; Wang, X. B.; Pickett, C. J.; Wang, L. S. J.; *J. Phys. Chem. A*, **2003**, *107*, 4612

[6] Teo, B. K.; Hall, M. B.; Fenske, R. F.; Dahl, L. F.; *Inorg. Chem.* **1975**, *14*, 3103

[7] DeKock, L. R.; Baerends, E. J.; Oskam, A.; *Inorg. Chem.* **1983**, *22*, 4158;

[8] DeKock, L. R.; Baerends, Hengelmolen, R.; *Organometallics* **1984**, *3*, 289

[9] Borg, S. J.; Behrsing, T.; Best, S. P.; Razavet, M.; Liu, X.; Pickett, C. J. *J. Am. Chem. Soc* **2004**, *126*, 16988

[10] Tye, J.W.; Darensbourg, M. Y.; Hall, M.B.; *J. Comput. Chem.* **2006**, *27*, 1454

[11] BP86 CO stretching mode frequency are not scaled by the usual 0.9914 factor (Cramer, C. J. Essentials of computational chemistrys - Theories and models; Wiley: New York, 2002.) because such scaling involves a worsening of the computed values with respect to the experimental values. B3LYP values are scaled using the 0.9614 factor (see ref.10)

[12] Georgakaki, I.; P.; Thomson, L.; M.; Lyon, E.; J.; Hall, M.; B.; Darensbourg, M.; Y.; *Coord. Chem. Rev.* **2003**, *238-239*, 255